Astron. Astrophys. 340, 371–380 (1998)

ASTRONOMY AND ASTROPHYSICS

Polarization properties of a sample of broad absorption line and gravitationally lensed quasars⋆,⋆⋆

D. Hutsemékers⋆⋆⋆, H. Lamy, and M. Remy

Institut d'Astrophysique, Université de Liège, 5 av. de Cointe, B-4000 Liège, Belgium

Received 20 July 1998 / Accepted 29 September 1998

Abstract. New broad-band linear polarization measurements have been obtained for a sample of 42 optically selected QSOs including 29 broad absorption line (BAL) QSOs. The polarization properties of different sub-classes have been compared, and possible correlations with various spectral indices searched for.

The main results of our study are: (1) Nearly all highly polarized QSOs of our sample belong to the sub-class of BAL QSOs with low-ionization absorption features (LIBAL QSOs). (2) The *range* of polarization is significantly larger for LIBAL QSOs than for high-ionization (HI) BAL QSOs and non-BAL QSOs. (3) There is some indication that HIBAL QSOs as a class may be more polarized than non-BAL QSOs and therefore intermediate between LIBAL and non-BAL QSOs, but the statistics are not compelling from the sample surveyed thus far. (4) For LIBAL QSOs, the *continuum* polarization appears significantly correlated with the *line profile* detachment index, in the sense that LIBAL QSOs with P Cygni-type profiles are more polarized. No correlation was found with the strength of the low- or the high-ionization absorption features, nor with the strength or the width of the emission lines.

These results are consistent with a scenario in which LIBAL QSOs constitute a different class of radio-quiet QSOs with more absorbing material and more dust. Higher maximum polarization can therefore be reached, while the actually measured polarization depends on the geometry and orientation of the system as do the line profiles. The observed correlation is interpreted within the framework of recent "wind-from-disk" models.

Key words: polarization – galaxies: quasars: absorption lines – galaxies: quasars: general – cosmology: gravitational lensing

1. Introduction

Broad absorption line quasi-stellar objects (BAL QSOs) are characterized by the presence in their spectra of broad, often deep, absorption troughs in the resonance lines of highly-ionized species like C IV, Si IV, or N V. These BALs appear blueshifted with respect to the corresponding emission lines. They are generally attributed to the ejection of matter at very high velocities ($\sim$0.1 c). About 12% of optically selected QSOs have BALs in their spectra, although this fraction could be underestimated if at least some BAL QSOs have their continuum more attenuated than non-BAL QSOs (Goodrich 1997). Apparently all BAL QSOs are radio-quiet[1] (Stocke et al. 1992). A recent account of BAL QSO properties may be found in Arav et al. (1997).

The fact that the broad emission line properties are essentially similar for BAL and non-BAL QSOs suggests that all radio-quiet QSOs could have a BAL region (BALR) of small covering factor, the BAL QSOs themselves being those objects with the BALR along the line of sight (e.g. Weymann et al. 1991, hereafter WMFH). Alternately, BAL and non-BAL QSOs may constitute two physically distinct populations of objects, BAL QSOs possibly representing an early stage in an evolutionary process towards normal QSOs (e.g. Boroson & Meyers 1992).

As first noticed by Stockman, Moore & Angel (1984), a number of BAL QSOs show high optical polarization ($\geq$ 3%) in the continuum while other radio-quiet QSOs (i.e. non-BAL ones) have generally low polarization ($\leq$ 1%). This important result has been recently confirmed by Hines & Schmidt (1997) on the basis of a larger sample. The fact that there is little or no variability of the polarization clearly distinguishes BAL QSOs from the so-called blazars. Since polarization is sensitive to the geometry of the objects (without spatially resolving them), a detailed understanding of BAL QSO polarization properties may provide important clues on the nature of the outflows and the status of these objects among AGN.

In this view, we have started a systematic polarimetric study of BAL QSOs. The present paper is devoted to the analysis of new broad-band polarization measurements obtained for a sam-

⋆ Tables 2 and 3 are also available in electronic form at the CDS via anonymous ftp to cdsarc.u-strasbg.fr (130.79.128.5) or via http://cdsweb.u-strasbg.fr/Abstract.html

⋆⋆ Based on observations collected at the European Southern Observatory (ESO, La Silla)

⋆⋆⋆ Also, Chercheur Qualifié au Fonds National de la Recherche Scientifique (FNRS, Belgium)

[1] There is only one known candidate radio-loud BAL QSO, 1556+3517, recently discovered by Becker et al. (1997). But Clavel (1998) finds that its radio-loudness is marginal after correcting for reddening

ple of 29 BAL QSOs, to which a number of normal radio-quiet QSOs have been added for comparison. Since an important issue is the study of possible correlations between polarization and other spectral characteristics, the objects have been essentially picked out from the WMFH sample which provides many useful quantitative spectral indices. Further, at least one BAL QSO is known to be gravitationally lensed. Its polarization could then be affected or induced by microlensing effects, i.e. by the selective magnification of some regions. We have therefore added to our sample several gravitationally lensed non-BAL QSOs with the aim of detecting any possible polarization difference.

The paper is organized as follows: the observing strategy and techniques are described in Sect. 2, as well as the methods for reducing the data and extracting accurate measurements. Instrumental polarization and de-biasing are also discussed in this section. In Sect. 3, the final sample of observed objects is detailed, sub-classes are defined, and several quantities characterizing the optical spectra are presented. Results are given in Sect. 4, including correlation searches between the various quantities. Conclusions and discussion form the last section.

2. Polarimetric observations and data reduction

The polarimetric observations were carried out on March 14–17 and September 3–6, 1994, at the European Southern Observatory (ESO La Silla, Chile), using the 3.6m telescope equipped with the EFOSC1 camera and spectrograph. The detector was a 512×512 TeK CCD (ESO#26) with a pixel size of 27 μm corresponding to $0''.605$ on the sky.

With EFOSC1, polarimetry is performed by inserting in the parallel beam a Wollaston prism which splits the incoming light rays into two orthogonally polarized beams. Each object in the field has therefore two images on the CCD detector, separated by about $20''$ and orthogonally polarized. To avoid image overlapping, one puts at the telescope focal plane a special mask made of alternating transparent and opaque parallel strips whose width corresponds to the splitting. The object is positioned at the centre of a transparent strip which is imaged on a region of the CCD chosen as clean as possible. The final CCD image then consists of alternate orthogonally polarized strips of the sky, two of them containing the polarized images of the object itself (Melnick et al. 1989, di Serego Alighieri 1989).

In order to derive linear polarization measurements, i.e. the two normalized Stokes parameters q and u, frames must be obtained with at least two different orientations of the Wollaston prism. This was done by rotating the whole EFOSC1 instrument by 45° (usually at the adapter angles 270° and 225°). For each object, two frames are therefore obtained. Typical exposure times are around 600s per frame, generally split into two shorter exposures. All observations were done with the Bessel V filter (ESO#553). The seeing was typically between $1''$ and $2''$, and the nights were photometric most of the time. Note that the polarization measurements do not depend on variable transparency or seeing since the two orthogonally polarized images of the object are simultaneously recorded. Finally, polarimetric calibration stars were observed (HD90177, HD161291, and HD164740; Schwarz 1987) in order to unambiguously fix the zero-point of the polarization position angle and to check the whole observing and reduction process.

Considering the two frames obtained with the instrument rotated at 270° and 225°, the normalized Stokes parameters are given by

$$q = \frac{I^1_{270} - I^2_{270}}{I^1_{270} + I^2_{270}}, \qquad u = \frac{I^1_{225} - I^2_{225}}{I^1_{225} + I^2_{225}}, \tag{1}$$

where I^1 and I^2 respectively refer to the intensities integrated over the two orthogonally polarized images of the object, background subtracted (Melnick et al. 1989). At this stage, the sign of q and u is arbitrary. It is clear from these relations that intensities must be determined with the highest accuracy. For this, the data were first corrected for bias and dark emission, and flat-fielded. A plane was locally fitted to the sky around each object image, and subtracted from each image individually. Since it appeared that standard aperture photometry was not accurate enough due to the rather large pixel size, we have measured the object center at subpixel precision by fitting a 2D gaussian profile and integrated the flux in a circle of same center and arbitrary radius by taking into account only those fractions of pixels inside the circle. With this method, the Stokes parameters may be computed for any reasonable radius of the aperture circle. They were found to be stable against radius variation, giving confidence in the method. In order to take as much flux as possible with not too much sky background, we finally fixed the aperture radius at $2.5\,(2\,\ln 2)^{-1/2}$ HW, where HW is the mean half-width at half-maximum of the gaussian profile. Note that in the few cases where the objects are resolved into multiple components, we use the smallest square aperture encompassing all the components. The whole procedure has been implemented within the ESO MIDAS reduction package. Applied to calibration stars, it provides polarization measurements in good agreement with the tabulated values. The zero-point of the polarization position angle is also determined from these stars, and the sign of q and u accordingly fixed. The uncertainties σ_q and σ_u are evaluated by computing the errors on the intensities I^1 and I^2 from the readout noise and from the photon noise in the object and the sky background (after converting the counts in electrons), and then by propagating these errors in Eq. 1. Uncertainties are typically around 0.15% for both q and u.

Since on most CCD frames field stars are simultaneously recorded, one can in principle use them to estimate the instrumental polarization, and to correct frame-by-frame the quasar Stokes parameters, following a method described by di Serego Alighieri (1989). However, the field stars (even when combined in a single "big" one per frame) are often fainter than the quasar, and a frame-by-frame correction introduces uncertainties on the quasar polarization larger than the instrumental polarization itself. Therefore, we tried to empirically correlate the instrumental polarization with observational parameters like the observing time or the position of the telescope, in order to check for possible variation and/or to derive a useful relation. Since no significant variation was found, we have finally computed the weighted average and dispersion of the normalized Stokes pa-

Table 1. Instrumental polarization

Date	$\overline{q}_\star$ (%)	$\sigma_{q_\star}$ (%)	$\overline{u}_\star$ (%)	$\sigma_{u_\star}$ (%)
03/94	+0.02	0.18	−0.10	0.34
09/94	+0.16	0.24	−0.30	0.29

rameters of field stars (a single "big" one per frame) considering all frames obtained during a given run. These values are given in Table 1. They indicate that the instrumental polarization is small. We take it into account in a rather conservative way by subtracting the systematic $\overline{q}_\star$ and $\overline{u}_\star$ from the quasar q and u, and by adding quadratically the errors. The final, corrected, values of the normalized Stokes parameters q and u are given in Table 2, together with the uncertainties. Note that possible contamination by interstellar polarization is included in the uncertainties (see also Sect. 4.1).

Then, from these values, the polarization degree is evaluated with $p = (q^2 + u^2)^{1/2}$, while the polarization position angle θ is obtained by solving the equations $q = p\cos 2\theta$ and $u = p\sin 2\theta$. The error on the polarization degree is estimated by $\sigma_p = (\sigma_q + \sigma_u)/2$, although the complex statistical behavior of the polarization degree should be kept in mind (Serkowski 1962, Simmons & Stewart 1985). Indeed, since p is always a positive quantity, it is biased at low signal-to-noise ratio. A reasonably good estimator of the true polarization degree, noted p_0, is computed from p and σ_p using the Wardle & Kronberg (1974) method (Simmons & Stewart 1985). Finally, the uncertainty of the polarization position angle θ is estimated from the standard Serkowski (1962) formula where p_0 is used instead of p to avoid biasing, i.e. $\sigma_\theta = 28\overset{\circ}{.}65\,\sigma_p/p_0$. All these quantities are given in Table 2. Also reported are the redshift z of the objects, the quasar sub-type (cf. Sect. 3.1), and $p_{\rm ISM}$, an upper limit to the galactic interstellar polarization along the object line of sight (cf. Sect. 4.1)

3. The observed sample and its characteristics

The observed QSOs were essentially chosen from the WMFH sample, which is a set of BAL and non-BAL QSOs from the Large Bright Quasar Survey (LBQS, cf. Hewett et al. 1995), augmented by several BAL QSOs from other sources. The selection was achieved during the observations depending on the QSO observability (position on the sky) and magnitude (priority to the brighter objects). A priority was also given to the BAL QSOs with low-ionization features. Five objects observable in the southern sky were added: 3 BAL QSOs from the Hartig & Baldwin (1986, hereafter HB) sample (0254-3327, 0333-3801, 2240-3702), and 2 non-BAL QSOs from the LBQS (2114-4346, 2122-4231). Finally, an additional 7 true or possible gravitationally lensed optically selected QSOs (cf. the compilation by Refsdal & Surdej 1994) were included in the sample.

The final sample then consists of 42 moderate to high redshift optically selected QSOs (cf. Tables 2 & 3). It contains 29 BAL QSOs, 12 non-BAL QSOs, and 1 "intermediate" object (2211-1915, cf. WMFH). 8 of them are true or possible gravitationally lensed QSOs, including 2 BAL QSOs: 1413+1143 and 1120+0154[2].

Among the 42 optically selected QSOs, 36 are definitely radio-quiet while only 1 is radio-loud (2211-1915, the "intermediate" object) (Stocke et al. 1992, Hooper et al. 1995, Véron & Véron 1996, Djorgovski & Meylan 1989, Bechtold et al. 1994, Reimers et al. 1995). The 5 remaining objects (3 BAL QSOs and 2 non-BAL QSOs: 0333-3801, 0335-3339, 2154-2005, 2114-4346, 2122-4231) have apparently not been measured at radio-wavelengths. However, they are most probably radio-quiet too (Stocke et al. 1992, Hooper et al. 1995).

3.1. The low-ionization BAL QSOs

Approximately 15% of BAL QSOs have deep low-ionization BALs (Mg II λ 2800 and/or Al III λ 1860) *in addition* to the usual high-ionization BAL troughs (WMFH, Voit et al. 1993). These objects might be significantly reddened by dust (Sprayberry & Foltz 1992). They also possibly constitute a physically different class of BAL QSOs (Boroson & Meyers 1992).

While objects with strong low-ionization (LI) features are recognized as LIBAL QSOs by most authors, the classification of objects with weaker features is controversial. We therefore define three categories of LIBAL QSOs: strong (S), weak (W), and marginal (M) LIBAL QSOs. The strong and weak LIBAL QSOs in our sample were all considered and first classified as such by WMFH. The strong ones are 0059-2735, 1011+0906, 1232+1325 and 1331-0108; the weak ones are 0335-3339, 1231+1320, 2225-0534 and 2350-0045 (WMFH "a" parameter < 1). But the classification by WMFH is rather conservative and includes only clear LIBAL QSOs, while several authors have reported faint LIBAL features in a number of other objects. We classify the latter objects as marginal LIBAL QSOs. These are 0043+0048, 1246-0542 and 2240-3702 (HB), 1413+1143 (Hazard et al. 1984, Angonin et al. 1990), 1120+0154 (Meylan & Djorgovski 1989), and 1212+1445 (this work). The marginal LIBAL QSOs are characterized by very weak Mg II and/or Al III BALs. The asymmetry of the Mg II or C III] emission lines, when cut on the blue side, is also considered as evidence for marginal LIBALs. Note finally that line strengths may be variable in some objects and that weak LIBALs could have been observed only once (namely due to possible microlensing effects as suspected in e.g. 1413+1143; Angonin et al. 1990, Hutsemékers 1993).

The remaining BAL QSOs are classified as high ionization (HI) only, except 0903+1734 and 1235+0857 which are unclassified, the Mg II line being outside the observed spectral range and no Al III BAL being detected. These classifications are summarized in Tables 2 and 3. Note that most spectra available in the literature were carefully re-inspected to check for the consistency of the classification. Altogether, the strong, weak and marginal LIBAL QSOs constitute approximately 50% of our

[2] Note that 1120+0154 = UM425 was only recently recognized as a BAL QSO (Michalitsianos & Oliversen 1995)

Table 2. Polarimetric results

Object	z	Type	q (%)	σ_q (%)	u (%)	σ_u (%)	p (%)	σ_p (%)	p_0 (%)	$p_{\rm ISM}$ (%)	θ (°)	σ_θ (°)
0006+0230	2.096	10	0.04	0.27	−0.10	0.31	0.11	0.29	0.00	0.08	145	–
0013−0029	2.084	10	−0.65	0.30	−0.79	0.35	1.03	0.33	0.97	0.07	115	10
0019+0107	2.124	20	0.13	0.27	0.88	0.30	0.89	0.29	0.85	0.10	41	10
0021−0213	2.296	20	0.65	0.30	−0.25	0.34	0.70	0.32	0.63	0.17	170	14
0025−0151	2.072	20	−0.37	0.26	0.24	0.31	0.44	0.28	0.37	0.15	74	22
0029+0017	2.226	20	0.54	0.32	−0.52	0.35	0.75	0.34	0.68	0.10	158	14
0043+0048	2.141	50	−0.14	0.27	−0.07	0.31	0.16	0.29	0.00	0.02	103	–
0059−2735	1.594	30	1.56	0.26	−0.44	0.31	1.62	0.29	1.60	0.16	172	5
0137−0153	2.232	20	−0.61	0.27	0.94	0.31	1.12	0.29	1.08	0.08	61	8
0142−1000	2.719	11	0.00	0.29	−0.28	0.33	0.28	0.31	0.00	0.08	135	–
0145+0416	2.029	20	−0.42	0.30	−2.67	0.34	2.70	0.32	2.68	0.21	131	3
0254−3327	1.862	20	−0.20	0.36	−0.02	0.40	0.20	0.38	0.00	0.04	93	–
0333−3801	2.210	20	0.01	0.26	0.83	0.30	0.83	0.28	0.78	0.00	45	10
0335−3339	2.258	40	0.02	0.33	0.60	0.35	0.60	0.34	0.53	0.00	44	19
0903+1734	2.776	60	−0.47	0.21	0.80	0.36	0.93	0.29	0.88	0.12	60	9
1009−0252	2.745	11	0.94	0.22	−0.07	0.38	0.95	0.30	0.90	0.07	178	9
1011+0906	2.262	30	0.60	0.23	−2.04	0.37	2.12	0.30	2.10	0.06	143	4
1029−0125	2.038	20	−0.54	0.24	−0.99	0.38	1.13	0.31	1.09	0.21	121	8
1104−1805	2.303	11	0.18	0.20	0.24	0.35	0.30	0.27	0.17	0.27	27	45
1115+0802	1.722	11	−0.02	0.19	0.68	0.35	0.68	0.27	0.63	0.17	46	12
1120+0154	1.465	51	1.84	0.19	0.63	0.35	1.95	0.27	1.93	0.17	9	4
1146+0207	2.055	10	0.22	0.25	−0.42	0.39	0.47	0.32	0.39	0.08	149	23
1208+1011	3.803	11	−0.18	0.24	0.30	0.37	0.35	0.30	0.23	0.00	60	38
1208+1535	1.956	20	−0.17	0.36	−0.11	0.47	0.20	0.42	0.00	0.28	107	–
1212+1445	1.621	50	0.98	0.23	1.06	0.36	1.45	0.30	1.42	0.25	24	6
1231+1320	2.386	40	0.59	0.25	−0.45	0.39	0.74	0.32	0.68	0.10	162	14
1232+1325	2.363	30	−1.95	0.30	−0.53	0.40	2.02	0.35	1.99	0.11	98	5
1235+0857	2.885	60	1.68	0.22	1.55	0.37	2.29	0.29	2.27	0.00	21	4
1246−0542	2.222	50	0.35	0.20	−0.84	0.36	0.91	0.28	0.87	0.07	146	9
1309−0536	2.212	20	0.78	0.21	−0.03	0.36	0.78	0.28	0.73	0.13	179	11
1331−0108	1.867	30	1.01	0.27	1.59	0.35	1.88	0.31	1.86	0.09	29	5
1413+1143	2.542	51	−0.78	0.25	1.32	0.36	1.53	0.31	1.50	0.00	60	6
1429−0053	2.084	11	0.95	0.18	0.31	0.40	1.00	0.29	0.96	0.18	9	9
1442−0011	2.215	20	0.16	0.22	−0.18	0.37	0.24	0.30	0.00	0.25	156	–
2114−4346	2.041	10	−0.11	0.29	−0.22	0.34	0.24	0.31	0.00	0.15	122	–
2122−4231	2.266	10	−0.01	0.27	−0.12	0.31	0.12	0.29	0.00	0.17	133	–
2154−2005	2.028	20	0.26	0.26	−0.70	0.30	0.75	0.28	0.69	0.07	145	12
2211−1915	1.951	10	0.14	0.27	0.03	0.31	0.14	0.29	0.00	0.08	6	–
2225−0534	1.981	40	3.58	0.27	−2.51	0.31	4.37	0.29	4.36	0.33	162	2
2230+0232	2.147	10	−0.36	0.28	−0.57	0.31	0.68	0.29	0.62	0.38	119	14
2240−3702	1.835	50	0.92	0.26	1.88	0.30	2.10	0.28	2.08	0.00	32	4
2350−0045	1.626	40	−0.58	0.27	−0.16	0.31	0.60	0.29	0.53	0.24	98	16

Object Type: First digit: (1) non-BAL QSOs + one intermediate object, (2) HIBAL QSOs, (3) Strong LIBAL QSOs, (4) Weak LIBAL QSOs, (5) Marginal LIBAL QSOs, (6) unclassified BAL QSOs; Second digit: (1) objects identified as true or possible gravitationally lensed QSOs

BAL QSO sample (but this is not representative of the actual proportion of LIBAL QSOs among BAL QSOs since priority was given to these objects).

3.2. The BAL QSO spectral characteristics

WMFH provide a series of spectral indices characterizing the absorption and emission features of BAL QSOs. For the absorption lines, they define the balnicity index (BI, in km s^{-1}) which is a modified velocity equivalent width of the C IV BAL, and the detachment index (DI, unitless) which measures the onset velocity of the strongest C IV BAL trough in units of the adjacent emission line half-width, that is, the degree of detachment of the absorption line relative to the emission one (see also HB who first distinguish between detached and P Cygni-type BAL profiles). Estimates of BI are also given by Korista et al. (1993) for most objects of our sample, such that we adopt for BI an average of these values and those from WMFH. WMFH also

Table 3. BAL QSO spectral characteristics

Object	Type	BI	DI	C IV HW	C III] HW	C IV EW	C III] EW	Fe II 2400 EW	Fe II 2070 EW	$\alpha_{\rm B}$	$\alpha_{\rm R}$
0019+0107	20	2305	4.65	1432	4193	7.5	18.1	21.99	5.96	0.73	0.68
0021−0213	20	5180	3.14	3077	3856	7.7	17.2	46.74	3.56	0.66	0.68
0025−0151	20	2878	2.97	1645	2528	10.9	23.4	19.90	1.96	0.34	1.07
0029+0017	20	5263	2.45	1857	3219	15.1	31.7	27.34	4.99	0.55	1.13
0043+0048	50	4452	10.06	987	1586	2.8	12.5	44.66	4.80	−0.13	0.77
0059−2735	30	11054	1.18	–	–	–	–	40.91	8.36	1.50	1.59
0137−0153	20	4166	2.41	1935	3125	8.2	22.6	35.95	6.32	1.01	1.26
0145+0416	20	4765	3.96	2341	–	12.5	–	33.10	5.36	0.96	0.42
0254−3327	20	694	1.08	1640	3125	8.1	22.5	23.00	2.40	0.64	0.91
0333−3801	20	3432	3.28	5450	3063	7.5	6.3	37.00	6.60	0.56	0.07
0335−3339	40	7460	15.90	599	–	1.7	–	95.66	14.16	1.91	1.74
0903+1734	60	9776	4.34	1548	5630	4.7	26.5	–	4.90	1.54	0.59
1011+0906	30	5587	6.84	3232	3754	7.9	11.1	40.91	9.16	1.95	1.51
1029−0125	20	1849	2.22	1645	3400	8.0	23.2	42.96	4.41	0.83	1.47
1120+0154	51	415	0.79	1343	–	8.5	–	–	–	0.45	1.25
1208+1535	20	4545	4.64	2709	5222	6.3	24.0	23.98	6.92	0.42	1.06
1212+1445	50	3619	6.05	1741	2363	3.8	4.9	25.29	3.37	1.51	1.08
1231+1320	40	3473	6.38	2612	4492	7.5	18.6	42.59	7.19	2.15	0.22
1232+1325	30	12620	1.84	3870	7123	17.5	42.9	58.76	11.80	2.38	0.92
1235+0857	60	815	0.42	1296	3840	10.4	24.0	–	3.00	1.04	0.45
1246−0542	50	4309	6.60	1587	3699	4.8	20.1	44.29	4.21	1.84	0.88
1309−0536	20	5363	5.10	3812	5128	8.1	23.7	36.42	5.19	1.41	0.90
1331−0108	30	7912	1.15	1935	3212	6.2	13.8	18.07	6.95	2.66	1.62
1413+1143	51	6621	1.50	1683	2937	18.8	35.0	–	1.89	1.72	0.63
1442−0011	20	5143	2.83	3522	5481	14.6	20.0	25.81	4.12	0.58	1.16
2154−2005	20	963	6.42	2438	3392	11.3	26.9	21.91	4.47	0.41	0.62
2225−0534	40	7903	0.48	1509	3251	11.3	43.4	53.38	7.67	1.68	2.21
2240−3702	50	8539	0.69	1940	3000	7.7	16.2	–	3.80	1.08	1.40
2350−0045	40	6964	5.08	1761	–	14.3	–	54.78	5.71	1.01	1.03

Object Type: First digit: (2) HIBAL QSOs, (3) Strong LIBAL QSOs, (4) Weak LIBAL QSOs, (5) Marginal LIBAL QSOs, (6) unclassified BAL QSOs; Second digit: (1) objects identified as true or possible gravitationally lensed QSOs. Units are given in the text

provide "clever" half-widths at half-maximum (HW, in km s^{-1}) and equivalent widths (EW, in Å) for the C IV, C III] and Fe II emission lines. For a more detailed definition of these indices, see WMFH.

For a few objects (0254-3327, 0333-3801, 2240-3702, and 1120+0154), some spectral indices were not provided. We therefore computed them using C IV spectra published by Korista et al. (1993) and Steidel & Sargent (1992). The spectra were digitally scanned, and the measurements done following the prescriptions given by WMFH. The measurements were also done for spectra of objects with published indices: a good agreement was found, giving confidence in our new values. For the C III] and Fe II emission lines, half-widths and equivalent widths were simply rescaled from those measured by HB. All these quantities are reported in Table 3.

In addition, we have evaluated the slope of the continuum using BAL QSO spectra digitally scanned from the papers by WMFH, HB, and Steidel & Sargent (1992). After some trials, we realized that some spectra cannot be easily fitted with a single power-law continuum: the slope often breaks roughly near C III], probably due to reddening and/or extended Fe II emission (compare for example the spectra of 1246-0542 and 1442-0011 in WMFH). We therefore decided to fit the continuum blueward and redward of C III], independently. The derived slopes $\alpha_{\rm B}$ and $\alpha_{\rm R}$ are given in Table 3, assuming a power-law continuum $F_\nu \propto \nu^{-\alpha}$. The values of $\alpha_{\rm B}$ and $\alpha_{\rm R}$ are affected by large uncertainties (not smaller than $\Delta\alpha \sim 0.3$), mainly due to the difficulty to accurately identify the continuum when the BALs are very large, when the Fe II emission/absorption is strong, or when the Mg II absorption is wide.

4. The results

4.1. Contamination by interstellar polarization

Since all objects in the sample are at high galactic latitudes ($|b_{\rm II}| > 35°$), the contamination by interstellar polarization in the Galaxy is expected to be negligible. This may be verified using the Burstein & Heiles (1982, hereafter BH) reddening maps[3]. The maps provide E(B-V) values from which the inter-

[3] The data files and routines were obtained from Schlegel 1998, via http://astro.berkeley.edu/davis/dust/data/bh/index.html

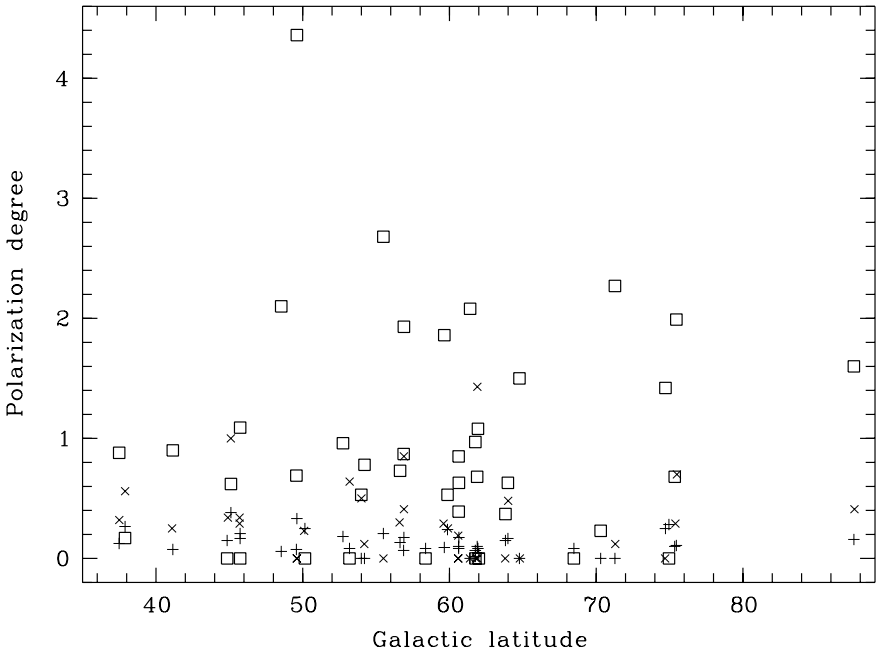

Fig. 1. The QSO polarization degree p_0 (in%) [□] is represented here as a function of the Galactic latitude of the objects ($|b_{II}|$, in degree), together with the de-biased polarization degree of field stars [×] (also corrected for the small systematic trend reported in Table 1), and the maximum interstellar polarization degree p_{ISM} derived from the Burstein & Heiles (1982) reddening maps [+]

stellar polarization is estimated with the relation $p_{ISM} \leq 8.3\%$ E(B-V) (Hiltner 1956). These upper limits on p_{ISM} are reported in Table 2. All but two are smaller than 0.3%, indicating a very small contamination by the Galaxy.

Polarization of faint field stars recorded on the CCD frames may also provide an estimate of the interstellar polarization. The dispersion of their Stokes parameters (Table 1) indicates that actually *both* instrumental and interstellar polarization are small. This is further illustrated in Fig. 1, where the QSO polarization is compared to the field star polarization (interstellar + instrumental), and to the maximum interstellar polarization derived from the BH maps. The absence of correlation between the field star polarization and the BH interstellar polarization suggests that instrumental polarization dominates field star polarization (although one cannot exclude that a few of them are intrinsically polarized). In addition, no deviation from uniformity was found in the distribution of the acute angle between quasar and field star polarization vectors measured on the same frame. These results confirm the insignificance of interstellar polarization in our sample.

We may therefore safely conclude that virtually any quasar with $p_0 \geq 0.5\%$ (or $p \geq 0.6\%$) is intrinsically polarized (cf. Fig. 1 and Table 1), in good agreement with the results obtained by Berriman et al. (1990) for low-polarization Palomar-Green (PG) QSOs.

4.2. Polarization variability

For some BAL QSOs of our sample, previous polarimetric measurements are available in the literature, and may be used for comparison. In Table 4, we list first epoch measurements obtained in 1977–1981. For all these objects, and within the limits of uncertainty, the values of the polarization position angles are in excellent agreement with ours (Table 2).

Table 4. Previous polarimetric measurements

Object	Date	p (%)	σ_p (%)	θ (°)	σ_θ (°)
0019+0107	11-05-78	0.93	0.26	24	8
0043+0048	11-05-78	0.33	0.38	103	25
0145+0416	10-23-81	0.58	0.68	131	34
0254−3327	10-24-81	0.62	1.16	154	54
1246−0542	4-05-78	1.87	0.31	139	5
1309−0536	6-09-78	2.33	0.57	179	7
1413+1143	6-06-81	3.39	0.48	49	4
2225−0534	9-11-77	4.09	0.79	166	6

From Moore & Stockman 1981, 1984, and Stockman et al. 1984

On the contrary, our values of p are generally smaller than or equal to the previous ones. However variability cannot be invoked since the observed differences are most likely due to the fact that the old measurements were done in white light and using detectors more sensitive in the blue, i.e. in a wavelength range where polarization is suspected to be higher (cf. Stockman et al. 1984, and more particularly the case of 1246-0542). Note further that those objects with null polarization ($p \leq \sigma_p$) are identical, except 0145+0416 which we find significantly polarized. But 0145+0416 is also the only object in our sample not far from a bright star which might contaminate the measurements. Its variability can nevertheless not be excluded.

In conclusion, we find no evidence in our sample of BAL QSOs for the strong polarization variability (in degree or angle) which characterizes blazars, confirming on a larger time-scale the results of Moore & Stockman (1981). This does not preclude the existence of small variations like those reported by Goodrich & Miller (1995) for 1413+1143.

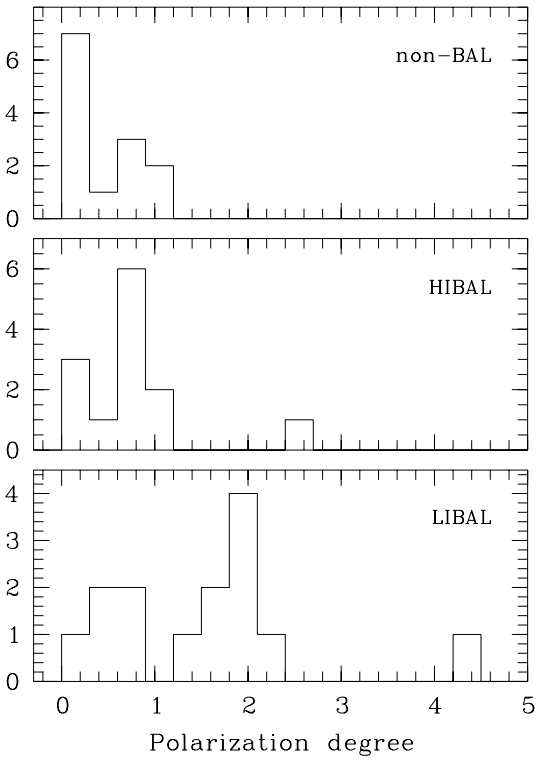

Fig. 2. The distribution of the polarization degree p_0 (in%) for the three main classes of QSOs. Non-BAL QSOs include the intermediate object. LIBAL QSOs contain the three sub-categories, i.e. strong, weak and marginal LIBAL QSOs

4.3. Polarization versus QSO sub-types

Before discussing the polarization properties of the different QSO sub-types, it is important to note that our sample is quite homogeneous in redshift (as from WMFH). Therefore, the polarization we measure in the V filter roughly refers to the same rest-frame wavelength range, such that differences between quasar sub-types will not be exaggerately masked by a possible wavelength dependence of the polarization. Also, spectral lines generally contribute little to the total flux in the V filter, and our polarimetric measurements largely refer to the polarization in the continuum.

Fig. 2 illustrates the distribution of p_0 for non-BAL, HIBAL and LIBAL QSOs. It immediately appears that nearly all QSOs with high polarization ($p_0 \geq 1.2\%$) are LIBAL QSOs. Only two other objects have high polarization (cf. Table 2): 1235+0857 which is unclassified (and therefore could be a LIBAL QSO), and 0145+0416 which has uncertain measurements (cf. Sect. 4.2). Also important is the fact that not all LIBAL QSOs do have high polarization (like 0335-3339 or 1231+1320 which are bona-fide ones; cf. WMFH and Voit et al. 1993). Further, although the strongest LIBAL QSOs are all highly polarized, there is apparently no correlation between the LIBAL strength and the polarization degree (cf. 2225-0534 or 1120+0154 which are weak and marginal LIBAL QSOs, respectively). This suggests that polarization is not systematically higher in LIBAL QSOs, but that its *range* is wider than in other QSOs. Although less polarized, several HIBAL QSOs also have intrinsic polarization ($p_0 \geq 0.5\%$), and apparently more often than non-BAL QSOs.

Table 5. Comparison of p_0 for various pairs of samples

Sample 1	Sample 2	n_1	n_2	$P_{\rm K-S}$
non-BAL	BAL	13	29	0.0253
non-BAL	LIBAL	13	14	0.0076
non-BAL	HIBAL	13	13	0.2914
non-BAL	HIBAL-	13	12	0.3973
LIBAL	HIBAL	14	13	0.0267
LIBAL	HIBAL-	14	12	0.0096
PG QSOs	non-BAL	88	13	0.1752
PG QSOs	BAL	88	29	0.0000
PG QSOs	LIBAL	88	14	0.0002
PG QSOs	HIBAL	88	13	0.0238
PG QSOs	HIBAL-	88	12	0.4282

The PG QSO sample is from Berriman et al. (1990), Seyfert galaxies and BAL QSOs excluded. HIBAL- refers to the HIBAL QSOs of our sample minus 0145+0416

The distribution of non-BAL QSOs peaks near $p_0 \sim 0\%$ with a mean value $< p_0 > \simeq 0.4\%$. It is in good agreement with the distribution found by Berriman et al. (1990) for low-polarization PG QSOs. The distribution of LIBAL QSOs is wider with a peak displaced towards higher polarization ($p_0 \sim 2\%$), and with $< p_0 > \simeq 1.5\%$. The distribution of HIBAL QSOs looks intermediate peaking near $p_0 \sim 0.7\%$, and with $< p_0 > \simeq 0.7\%$.

To see whether these differences are statistically significant, a two-sample Kolmogorov-Smirnov (K-S) statistical test (from Press et al. 1989) has been used to compare the observed distributions of p_0. In Table 5, we give the probability that the distributions of two sub-samples are drawn from the same parent population, considering various combinations. We also include a comparison with the polarization of PG QSOs (after de-biasing the polarization degrees as described in Sect. 2). The number of objects involved in the sub-samples (n_1 and n_2) are given in the table. The difference between LIBAL and non-BAL QSOs appears significant ($P_{\rm K-S} < 0.01$) as well as the difference between LIBAL and HIBAL QSOs. However, no significant difference between HIBAL and non-BAL QSOs can be detected. Comparison with PG QSOs confirms these results. It also suggests that the distributions of non-BAL, HIBAL, and PG QSOs do not significantly differ, although the latter objects have much lower redshifts and were measured in white light (any marginal difference with HIBAL QSOs is due to the polarization of 0145+0416, which is uncertain).

These results suggest that the polarization of LIBAL QSOs definitely differs from that of non-BAL and HIBAL QSOs, showing a distribution significantly extended towards higher polarization. On the contrary, no significant difference is found between HIBAL and non-BAL QSOs. The difference, if any, is small and would require a larger sample and more accurate measurements to be established.

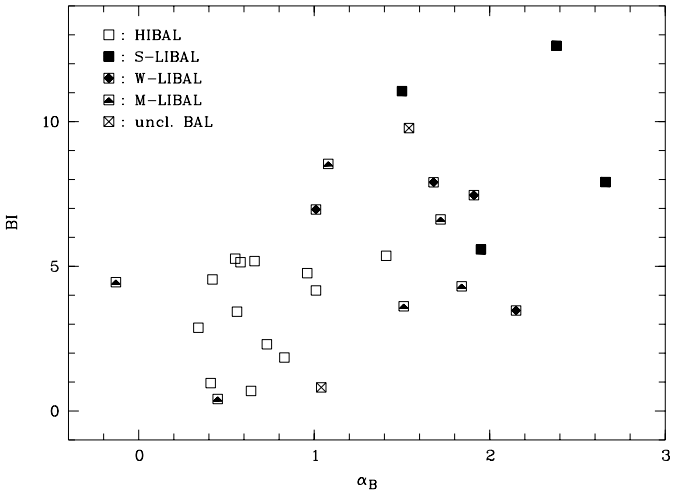

Fig. 3. The correlation between the balnicity index BI (in 10^3 km s^{-1}) and the slope of the continuum $\alpha_{\rm B}$ for all BAL QSOs of our sample

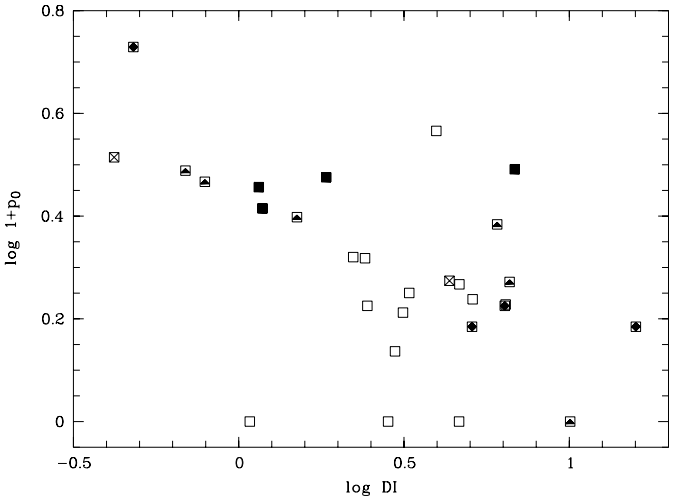

Fig. 4. The correlation between the polarization degree p_0 (in%) and the line profile detachment index DI for all BAL QSOs of our sample. Symbols are as in Fig. 3. The correlation is especially apparent for the QSOs of the LIBAL sample

Finally, no polarization difference was found when comparing the gravitationally lensed QSOs to other non-BAL or BAL QSOs. When polarized, their polarization is essentially related to their BAL nature. Small variations due to microlensing in either component can nevertheless be present (Goodrich & Miller 1995).

4.4. BAL QSO polarization versus spectral indices

The previous results suggesting a different behavior of LIBAL QSOs, it is important to recall that these QSOs also differ by the strength of their high-ionization features and the slope of their continuum (WMFH, Sprayberry & Foltz 1992). This is clearly seen in Fig. 3, using our newly determined continuum slopes. LIBAL QSOs (including several marginal ones) appear to have the highest balnicity indices and the most reddened continua. These differences are significant: the probability that the distribution of BI (resp. $\alpha_{\rm B}$) in HIBAL and LIBAL QSOs is drawn from the same parent population is computed to be $P_{\rm K-S}$ = 0.008 (resp. 0.002). In addition BI and $\alpha_{\rm B}$ seem correlated. Possible correlations may be tested by computing the Kendall (τ) and the Spearman (r_s) rank correlation coefficients (Press et al. 1989; also available in the ESO MIDAS software package). The probability P_τ that a value more different from zero than the observed value of the Kendall τ statistic would occur by chance among uncorrelated indices is P_τ = 0.003, for n = 29 objects. The Spearman test gives P_{r_s} = 0.001. This indicates a significant correlation between BI and $\alpha_{\rm B}$ in the whole BAL QSO sample.

Possible correlations between the polarization degree p_0 and the various spectral indices were similarly searched for by computing the Kendall τ and the Spearman r_s statistics. The resulting probabilities P_τ and P_{r_s} are given in Table 6, for the whole BAL QSO sample and for LIBAL QSOs only. Note that similar results are obtained when using p instead of p_0. From this table, it appears that the polarization degree is significantly correlated with the slope of the continuum $\alpha_{\rm B}$, and with the line profile detachment index DI.

Table 6. Analysis of correlation between p_0 and various indices

	BAL QSOs			LIBAL QSOs		
Index	P_τ	P_{r_s}	n	P_τ	P_{r_s}	n
BI	0.198	0.179	29	0.226	0.169	14
DI	0.007	0.014	29	0.004	0.009	14
C IV HW	0.968	0.857	28	0.158	0.158	13
C III] HW	0.880	0.845	24	0.325	0.405	10
C IV EW	0.334	0.331	28	0.075	0.078	13
C III] EW	0.546	0.612	24	0.325	0.446	10
Fe II 2400 EW	0.632	0.553	24	0.303	0.391	11
Fe II 2070 EW	0.358	0.321	28	0.667	0.571	13
$\alpha_{\rm B}$	0.007	0.004	29	0.582	0.459	14
$\alpha_{\rm R}$	0.393	0.375	29	0.061	0.086	14

The correlation with $\alpha_{\rm B}$ disappears when considering LIBAL QSOs only, although p_0 and $\alpha_{\rm B}$ still span a large range of values. Most probably, this correlation is detected in the whole BAL QSO sample as a consequence of the different distributions of both $\alpha_{\rm B}$ and p_0 in the LIBAL and HIBAL QSO sub-samples (Figs. 2 and 3).

On the contrary, the correlation with the detachment index holds for the whole BAL QSO sample as well as for the LIBAL QSO sub-sample. It is illustrated in Fig. 4. In fact, the correlation appears dominated by the behavior of LIBAL QSOs. HIBAL QSOs roughly follow the trend, but their range in DI is not large enough to be sure that they behave similarly[4]. It is interesting to remark that the observed correlation is stable – and even slightly better – if we assume that the polarization degree increases towards shorter wavelengths, i.e. if p_0 is redshift-dependent. This

[4] Note that the apparent difference between the distributions of DI for LIBAL and HIBAL QSOs is not significant ($P_{\rm K-S}$ = 0.179)

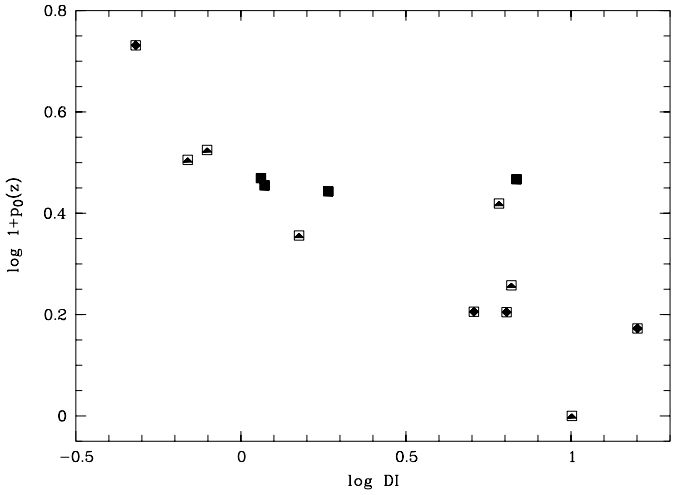

Fig. 5. The correlation between the redshift-corrected polarization degree $p_0(z)$ (in%) and the line profile detachment index DI for LIBAL QSOs only. We assume $p_0(z) = p_0(\frac{3}{1+z})$, i.e. a λ^{-1} dependence of p_0. Symbols are as in Fig. 3

is as illustrated in Fig. 5 for the LIBAL QSO sub-sample, assuming a reasonable λ^{-1} dependence (e.g. Cohen et al. 1995). In this case, P_τ = 0.0006 and P_{r_s} = 0.0003.

No other correlation of p_0, namely with the balnicity index, or with emission line indices is detected.

5. Discussion and conclusions

New broad-band linear polarization measurements have been obtained for a sample of 42 optically selected QSOs including 29 BAL QSOs (14 LIBAL and 13 HIBAL). The polarization properties of the different sub-classes have been compared, and possible correlations with various spectral indices searched for. The main results of our study are:

- Nearly all highly polarized QSOs of our sample belong to the LIBAL class (provided that BAL QSOs with weaker low-ionization features are included in the class).
- The *range* of polarization is significantly larger for LIBAL QSOs than for HIBAL and non-BAL QSOs. It extends from 0% to 4.4%, with a peak near 2%.
- There is some indication that HIBAL QSOs as a class may be more polarized than non-BAL QSOs and therefore intermediate between LIBAL and non-BAL QSOs, but the statistics are not compelling from the sample surveyed thus far.
- We confirm the fact that LIBAL QSOs (including weaker ones) have larger balnicity indices and more reddened continua than HIBAL QSOs.
- The *continuum* polarization appears correlated with the *line profile* detachment index, especially in the LIBAL QSO subsample.
- No correlation is found between polarization and the strength of the low- or the high-ionization absorption features, nor with the strength or the width of the emission lines. The apparent correlation between polarization and the slope of the continuum is probably due to the different distribution of these quantities within the HIBAL and LIBAL sub-samples.

The fact that LIBAL QSOs have different polarization properties is an additional piece of evidence that these objects could constitute a different class of radio-quiet QSOs, as suggested by several authors (WMFH, Sprayberry & Foltz 1992, and Boroson & Meyers 1992), HIBAL QSOs being much more similar to non-BAL QSOs. The higher maximum polarization observed in LIBAL QSOs is probably related to the larger amount of absorbing material and/or dust, either via the presence of additional scatterers (dust or electrons), or via an increased attenuation of the direct continuum.

The correlation between the continuum polarization and the detachment index was unexpected, especially since the latter index is a rather subtle characteristic of the line profiles which involves both absorption and emission components. The correlation is in the sense that LIBAL QSOs with detached C IV profiles are less polarized in the continuum, while those with P Cygni-type C IV profiles are more polarized. The most obvious explanation for such a correlation is that the high-ionization line profiles and the continuum polarization both depend on the geometry and/or the orientation of the LIBAL QSOs. This would explain that a range of polarization degrees is in fact observed, the maximum value being characteristic of the class. It is not excluded that HIBAL QSOs behave similarly within a smaller polarization range.

Murray et al. (1995) proposed a BAL flow model which accounts for many of the observed BAL profiles including the detached ones. Instead of being accelerated radially from a central source, the flow emerges from the accretion disk at some distance from the central source. It is then exposed to the continuum radiation and accelerated, rapidly reaching radial trajectories. The wind has naturally a maximum opening angle, and may produce polarization in the continuum via electron scattering. Other recent models are also based on such a "wind-from-disk" paradigm, and may result in roughly similar geometry and kinematics although acceleration mechanisms, photoionization, cloud size and filling factor could significantly differ (de Kool & Begelman 1995, Königl & Kartje 1994, Emmering et al. 1992).

Murray et al. (1995) show that for a flow seen nearly along the disk, P Cygni-type profiles with black troughs at low velocities are naturally produced. For the flow seen at grazing angle along the upper edge of the wind, high-velocity detached absorptions are obtained. Since the direct continuum is expected to be more attenuated for lines of sight near the disk, the continuum polarization is expected to be higher for orientations which produce P Cygni-type profiles than for orientations which produce detached profiles. This is in good qualitative agreement with the observed correlation. This mechanism has already been proposed by Goodrich (1997) to explain the higher polarization of some PHL5200-like (i.e. P Cygni-type) BAL QSOs. The polarization being uncorrelated with the slope of the continuum in the LIBAL QSO sub-sample, this differential attenua-

tion should be dominated by electron scattering in the wind. In fact, the electron scattering models of Brown & McLean (1977) also account for the observed behavior. For the cylindrical sector geometry which roughly characterizes the "wind-from-disk" models, Brown & McLean (1977) found that the observed polarization is given by $p \propto n_0 R \sin\phi \cos^2\phi \sin^2 i$, where i is the inclination of the system ($i = 0°$ for the disk in the plane of the sky), ϕ the opening half-angle of the wind, R its maximum extension, and n_0 a uniform electron density. With this geometry, polarization is higher along the equatorial line of sight (i = 90°) than along any other line of sight, again in good agreement with the observed correlation. In addition to this orientation effect within the LIBAL QSO sub-class, we see that the higher wind opacities (from either density or size) or the larger covering factors (up to $\phi \sim 35°$) which possibly distinguish LIBAL QSOs from HIBAL QSOs lead to higher maximum polarizations, as observed. While these models are certainly too simple to reproduce quantitatively the observations, the good overall agreement is encouraging.

A problem with the "wind-from-disk" model is that low-ionization features are assumed to be formed near the disk and therefore only observable for nearly equatorial lines of sight (Murray et al. 1995); low-ionization absorption troughs and high-ionization detached profiles are apparently mutually exclusive. Since this is not the case observationally, we have to admit that low-ionization features could form at large distance from the core also along inclined views. In this case, low-ionization features could be observed not only at the low-velocity end of the high-ionization troughs, but also at higher velocities. And indeed, more complex velocity structures are observed in the low-ionization troughs of two LIBAL QSOs with detached C IV profiles, 0335-3339 and 1231+1320 (Voit et al. 1993), giving some support to this hypothesis. Assuming more extended LIBAL regions would also imply that LIBAL and HIBAL QSOs are different objects, in agreement with other studies (e.g. Boroson & Meyers 1992). Possibly, the efficiency of the X-ray shielding could make the difference.

While unexpected a priori, the correlation found between LIBAL QSO line profiles and continuum polarization fits reasonably well the "wind-from-disk" models, without the need of ad-hoc explanations. Clearly, the possibility of more extended LIBAL regions should be investigated theoretically. More detailed polarization differences between objects with detached and with P Cygni-type profiles should be carefully investigated, namely using spectropolarimetry. Also, possible differences between the X-ray properties of LIBAL and HIBAL QSOs would be worthwhile to detect.

Acknowledgements. This research is supported in part by the contract ARC 94/99-178, and a project funded by SSTC/ Prodex. We would like to thank Jean Surdej for reading the manuscript, and the referee for useful comments.

References

Angonin M.C., Remy M., Surdej J., Vanderriest C., 1990, A&A 233, L5
Arav N., Shlosman I., Weymann R.J., 1997, Mass Ejection from Active Galactic Nuclei. ASP Conference Series 128, San Francisco
Bechtold J., Elvis M., Fiore F., et al., 1994, AJ 108, 374
Becker R.H., Gregg M.D., Hook I., et al., 1997, ApJ 479, L93
Berriman G., Schmidt G.D., West S.C., Stockman H.S., 1990, ApJS 74, 869
Boroson T.A., Meyers K.A., 1992, ApJ 397, 442
Brown J.C., McLean I.S., 1977, A&A 57, 141
Burstein D., Heiles C., 1982, AJ 87, 1165 (BH)
Clavel J., 1998, A&A 331, 853
Cohen M.H., Ogle P.M., Tran H.D., et al., 1995, ApJ 448, L77
de Kool M., Begelman M.C., 1995, ApJ 455, 448
di Serego Alighieri S., 1989, In: Grosbøl P.J. et al. (eds.) 1^{st} ESO/ST-ECF, Data Analysis Workshop, 157
Djorgovski S., Meylan G., 1989, In: Moran J.M. et al. (eds.) Gravitational Lenses. Lect. Notes Phys. 330, 173
Emmering R.T., Blandford R.D., Shlosman I., 1992, ApJ 385, 460
Goodrich R.W., Miller J.S., 1995, ApJ 448, L73
Goodrich R.W., 1997, ApJ 474, 606
Hartig G.F., Baldwin J.A., 1986, ApJ 302, 64 (HB)
Hazard C., Morton D.C., Terlevich R., McMahon R., 1984, ApJ 282, 33
Hewett P.C., Foltz C.B., Chaffee F.H., 1995, AJ 109, 1498
Hiltner W.A., 1956, ApJS 2, 389
Hines D.C., Schmidt G.D., 1997, In: Arav N. et al. (eds.) Mass Ejection from Active Galactic Nuclei. ASP Conference Series 128, 59
Hooper E.J., Impey C.D., Foltz C.B., Hewett P.C., 1995, ApJ 445, 62
Hutsemékers D., 1993, A&A 280, 435
Königl A., Kartje J.F., 1994, ApJ 434, 446
Korista K.T., Voit G.M., Morris S.L., Weymann R.J., 1993, ApJS 88, 357
Melnick J., Dekker H., D'Odorico S., 1989, EFOSC, ESO operating manual No 4, Version 2, ESO
Meylan G., Djorgovski S., 1989, ApJ 338, L1
Michalitsianos A.G., Oliversen R.J., 1995, ApJ 439, 599
Moore R.L., Stockman H.S., 1981, ApJ 243, 60
Moore R.L., Stockman H.S., 1984, ApJ 279, 465
Murray N., Chiang J., Grossman S.A., Voit G.M., 1995, ApJ 451, 498
Press W.H., Flannery B.P., Teukolsky S.A., Vetterling W.T., 1989, Numerical Recipes, Cambridge University Press
Refsdal S., Surdej J., 1994, Rep. Prog. Phys. 56, 117
Reimers D., Bade N., Schartel N., et al., 1995, A&A 296, L49
Schwarz H.E., 1987, In: Polarimetry with EFOSC. ESO Internal Memorandum Dec. 1987
Serkowski K., 1962, In: Kopal Z. (ed.) Advances in Astronomy and Astrophysics. Academic Press 1, 289
Simmons J.F.L., Stewart B.G., 1985, A&A 142, 100
Sprayberry D., Foltz C.B., 1992, ApJ 390, 39
Steidel C.C., Sargent W.L.W. 1992, ApJS 80, 1
Stocke J.T., Morris S.L., Weymann R.J., Foltz C.B., 1992, ApJ 396, 487
Stockman H.S., Moore R.L., Angel J.R.P., 1984, ApJ 279, 485
Véron M.-P., Véron P., 1996, A Catalogue of Quasars and Active Nuclei (7th Edition), ESO Scientific Report 17
Voit G.M., Weymann R.J., Korista K.T., 1993, ApJ 413, 95
Wardle J.F.C., Kronberg P.P., 1974, ApJ 194, 249
Weymann R.J., Morris S.L., Foltz C.B., Hewett P.C., 1991, ApJ 373, 23 (WMFH)